Exclusive studies of angular distributions in GeV hadron-induced reactions with ^{197}Au

W.-c. Hsi, K. Kwiatkowski,* G. Wang,† D. S. Bracken,* E. Cornell,‡ D. S. Ginger,§ and V. E. Viola
Departments of Chemistry, Physics and IUCF, Indiana University, Bloomington, Indiana 47405

R. G. Korteling
Department of Chemistry, Simon Fraser University, Burnaby, British Columbia, Canada V5A I56

K. B. Morley
Physics Division, Los Alamos National Laboratory, Los Alamos, New Mexico 87545

R. Huang, W. G. Lynch, M. B. Tsang, and H. Xi
Department of Physics and NSCL, Michigan State University, East Lansing, Michigan 48824

F. Gimeno-Nogues, E. Ramakrishnan, D. Rowland, and S. J. Yennello
Department of Chemistry and Cyclotron Institute, Texas A & M University, College Station, Texas 77843

H. Breuer
Department of Physics, University of Maryland, College Park, Maryland 20740

S. Gushue and L. P. Remsberg
Chemistry Department, Brookhaven National Laboratory, Upton, New York 11973

A. Botvina‖
Department of Physics, University of Bologna, Bologna I-40126, Italy

W. A. Friedman
Department of Physics, University of Wisconsin, Madison, Wisconsin 53706
(Received 28 April 1999; published 11 August 1999)

Exclusive studies of angular distributions for intermediate-mass fragments (IMFs) produced in GeV hadron-induced reactions have been performed with the Indiana Silicon Sphere (ISiS) 4π detector array. Special emphasis has been given to understanding the origin of sideways peaking, which becomes prominent in the angular distributions for beam momenta above about 10 GeV/c. Both the magnitude of the effect and the peak angle increase as a function of fragment multiplicity and charge. When gated on IMF kinetic energy, the angular distributions evolve from forward-peaked to near isotropy as the fragment kinetic energy decreases. Fragment-fragment angular-correlation analyses show no obvious evidence for a dynamic mechanism that might signal shock wave effects or the breakup of exotic geometric shapes such as bubbles or toroids. Moving-source and intranuclear cascade simulations suggest that the observed sideways peaking is of kinematic origin, arising from significant transverse momentum imparted to the heavy recoil nucleus during the fast cascade stage of the collision. A two-step cascade and statistical multifragmentation calculation is consistent with this assumption. [S0556-2813(99)02909-X]

PACS number(s): 25.40.Ve, 21.65.+f, 25.70.Pq, 25.75.−q

I. INTRODUCTION

The preferential emission of intermediate mass fragments (IMF: $3 \leqslant Z \lesssim 20$) at angles transverse to the beam axis, or sideways peaking, was indicated by emulsion and radiochemical studies over 30 years ago ([1,2] and references therein). Subsequent detector studies of 28-GeV proton-induced reactions with ^{197}Au and ^{238}U by Remsberg and Perry [3] showed that this was a general feature of IMF emission for high bombarding energies. This observation stands in sharp contrast to numerous measurements at energies below about 5 GeV, where the IMF angular distributions have been found to be distinctly forward-peaked [4–6].

Several radiochemical measurements by Porile [7], and Urbon and co-workers [8] demonstrated that the transition from forward to sideways peaking occurs between incident proton energies of 5–10 GeV. It is in the same energy interval that IMF cross sections [9] and deposition energy [10] become nearly independent of bombarding energy. In addi-

*Present address: Los Alamos National Lab, Los Alamos, NM 87545.
†Present address: Epsilon, Inc., Dallas, TX 75240.
‡Present address: Lawrence Berkeley Laboratory, Berkeley, CA 94720.
§Present address: Department of Physics, Cambridge University, Cambridge, United Kingdom.
‖On leave from Institute for Nuclear Research, RU-117312 Moscow, Russia.

tion, a distinct change in the character of the energy spectra is observed [9,11], signaling the onset of multifragmentation. In fact, above about 5 GeV incident proton energy, the angular distributions are the only IMF observable that appears to be sensitive to the beam energy.

The sideways-peaked nature of hadron-nucleus angular distributions at high energies suggests the possibility that dynamic effects associated with the initial cascade phase of the reaction might play an important role in the multifragmentation process. If so, this would negate some of the simplifying advantages of relativistic hadrons for nuclear equation-of-state investigations [10].

Several interpretations of the sideways-peaking phenomenon have been proposed. Remsberg and Perry [3] noted that the peak in the IMF angular distributions near 60°–70° coincided with the angular region predicted for light particles ejected from a nuclear shock wave [12,13]. Coalescence of nucleons along the shock-wave front would then lead to preferential emission of IMFs at these angles. Fortney and Porile [7] also suggested a one-step mechanism involving a coherent interaction between the incident proton and the Lorentz-contracted target nucleus in its path. Ejection of this material in the forward direction, plus additional mass loss in the vicinity of the interaction region, would produce a highly unstable nucleus that breaks apart normal to the beam axis. However, they also discuss a mechanism in which forward-emitted fast particles are accompanied by a heavy recoil nucleus emitted at backward angles to account for their results. In a similar vein, Wilkins *et al.* [14] and Hüfner [15] explained the observation of energetic fissionlike residues in terms of a nuclear cleavage model in which the leading hadron creates a cylindrical low-density region in its wake. Large transverse momentum transfer and Coulomb forces then act to focus the binary fragments transverse to the beam axis.

In contrast, Urbon *et al.* [8] were able to account for their IMF angular distribution results at 11.5 GeV with a two-step model involving a fast cascade followed by the decay of a hot residue. More recently, coincidence studies in a planar geometry with 12-GeV protons [16], showed that sideways peaking for heavier IMFs was enhanced when a second IMF was detected near 90° on the opposite side of the beam. It was suggested that this observation might be due to geometrical effects such as the breakup of a toroid-shaped nucleus, as predicted by a QMD calculation [17]. However, in order to reproduce the data, the calculation required adjustment of the parameters to values well outside the default values of the model.

Speculation concerning the stability of exotic nuclear shapes such as bubbles or toroids has existed for many years, following calculations by Siemens and Bethe [18] and Wong [19] and more recently in Refs. [20–22]. Recent Boltzmann-Uehling-Uhlenbeck (BUU) calculations [23] provide additional support for the possible role of dynamics and nuclear geometry in destabilizing heavy residues formed in central collisions induced by hadrons above about 5 GeV/c momentum. First, as the projectile and its associated momentum front punch through the nucleus, significant mass loss occurs, creating conditions favorable to development of an acoustic-type shock wave with low compression ($\rho/\rho_0 \sim 1.3$). Second, a significant depletion of nucleons in the nuclear core is predicted to evolve near the end of the fast cascade, creating a temporary bubblelike geometry in the hot residue with density ($\rho/\rho_0 \cong 0.7$), near the spinodal region. How the cohesive nuclear forces respond to these rapid perturbations and whether sideways peaking is a manifestation of such effects is a central question in distinguishing between dynamically-driven and thermal multifragmentation. This question has also been examined recently in the context of the intranuclear cascade model [24]. In this work we describe exclusive 4π studies that examine the sideways peaking phenomenon as a function of fragment correlation angles, multiplicity, charge and kinetic energy over a range of projectile energies spanning the transition region from forward-to-sideways peaking. Preliminary results have been published previously [25]. We first discuss the experimental measurements and then address the experimental evidence for the sideways-peaking effect. This is followed by an analysis of the data and a proposed explanation for the observations.

II. EXPERIMENTAL PROCEDURES

The experiment was performed with the Indiana Silicon Sphere (ISiS) 4π detector array [26] at the Brookhaven National Laboratory Alternating Gradient Synchrotron (AGS) accelerator. Untagged secondary positive beams of momentum 6.0, 10.0, 12.8 and 14.6 GeV/c and negative beams at 5.0, 8.2 and 9.2 GeV/c were incident on a ^{197}Au target. Average beam intensities were approximately 4×10^6 particles/cycle, with a cycle time of 4.3 seconds and flat top of 2.2 seconds. The composition of the positive beam, as indicated by AGS secondary production tables, ranged from about 90% proton/10% π^+ at the highest momentum to 60% proton/40% π^+ at the lowest momentum. The negative beam composition was predicted to be $>95\%$ π^-, a few percent K^- and less than 1% $\bar{p}$ for the momenta studied here. For the purposes of these discussions, we identify positive beam with protons and the negative beam with π^-. As has been shown in Ref. [10], the rationale for this assumption is based on the insensitivity of the charged-particle multiplicity distributions to beam momentum or hadron type in these experiments.

The ^{197}Au target foils were prepared from 10^{-5} purity metal by vacuum evaporation onto a glass slide, using a KCl substrate that was subsequently removed by repeated washing. Two targets, 1×1 cm^2 and 2×2 cm^2 in area and 1.8 mg/cm^2 in thickness, were used to define the beam-target geometry. In order to provide a self-supporting target with minimum extraneous material exposed to the beam halo, each target was supported by two 50 μm tungsten wires attached to a 50 mm$\times$50 mm target frame. A blank target was also inserted into the beam periodically to monitor the level of possible nontarget contributions to the spectra.

The ISiS detector array consists of 162 triple-detector telescopes arranged in a spherical geometry. The telescopes span the polar-angle range from 14°–86.5° in five segments in the forward hemisphere and 93.5°–166° in four backward-hemisphere segments. The azimuthal coverage consists of 18

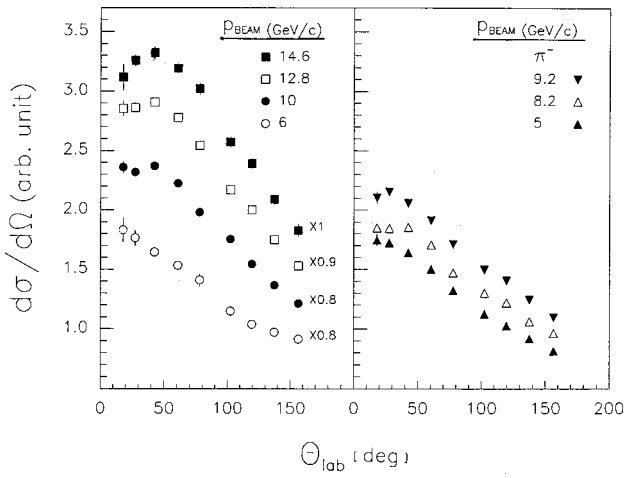

FIG. 1. ''Inclusive'' angular distributions of carbon fragments from a ^{197}Au target. The left frame gives the data for incident protons and the right frame shows the results for the π^- beam. Beam momenta are indicated in the figure.

telescopes in an annular ring, each subtending ~20° in azimuthal angle. The most forward ring is divided into two polar-angle segments. Total solid-angle coverage was 70% for the active telescopes in this experiment.

The detector telescopes consisted of a gas-ionization chamber operated at 16–18 Torr of C_3F_8 gas, a 500 μm passivated silicon detector, and a 28-mm *CsI* scintillator with photodiode readout. Details of the detector design are given in [26]. The energy acceptance for IMF charge identification was $1.0 \lesssim E/A \lesssim 90$ MeV. Isotope identification was possible for LCPs with $E/A > 8$ MeV (LCP: H and He isotopes). In addition, all ejectiles with energies $E \gtrsim 16$ MeV in the *CsI* detector (but with the *E* fast silicon signal too low to trigger the corresponding detector) were recorded for each accepted event, along with the recorded silicon linear signal. This provided information on the multiplicity of fast cascade ejectiles (primarily charged hadrons) with energies up to ~ 400 MeV. This definition corresponds approximately to that of ''gray particles'' observed in emulsion studies.

The hardware multiplicity trigger for event acceptance required valid fast signals in three or more silicon detectors in the array. Results with this minimum-bias hardware trigger are referred to as ''inclusive'' in this paper. The ISiS array was complemented by a 15 cm×15 cm upstream total beam counter (TB), an annular ring veto scintillator (RV), a 28 mm×28 mm beam-definition counter (BC), and a segmented inner/outer scintillator array (UV) upstream from the target for halo, veto and beam alignment. The acceptance trigger logic was $TB \cdot \overline{RV} \cdot BC \cdot \overline{UV} \cdot$ ISiS.

III. SIDEWAYS PEAKING: SHOCK WAVES? EXOTIC GEOMETRIES?

In Fig. 1 the ''inclusive'' angular distributions are shown for carbon fragments emitted in the seven systems studied in this work. These data are representative for all $Z \geqslant 5$ IMFs. The left-hand panel shows the data for the proton-induced reactions and the right-hand panel contains the π^- results.

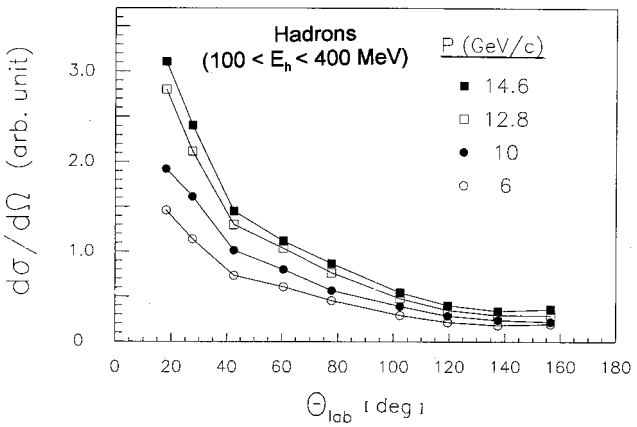

FIG. 2. ''Inclusive'' angular distributions for ''gray protons'' ($100 \leqslant Ep \leqslant 400$ MeV) emitted in proton-induced reactions on ^{197}Au. Beam momenta are indicated in the figure.

As the beam momentum increases, the evolution from forward to sideways peaking of the angular distributions is apparent, becoming a pronounced feature above beam energies of about 10 GeV/*c*. While even at 14.6 GeV/*c* the sideways peaking effect is small (~20%), it is nonetheless a systematic feature of all systems above 10 GeV/*c* [3,7–10].

If shock-wave-like effects are responsible for the sideways peaking of IMFs, similar peaking might be expected to appear in the LCP spectra. Figures 2 and 3 present ''inclusive'' angular distributions for, respectively, ''gray'' protons ($100 \leqslant E_H \leqslant 400$ MeV) and ^{3,4}He ions ($40 \leqslant E_{He} \leqslant 110$ MeV) observed for the four proton beam momenta. The proton yield is strongly forward-peaked for all momenta. The same is true for ^{4}He, although with a reduced forward-backward ratio compared to protons. For ^{3}He the slope of the angular distributions flattens out at forward angles, although no statistically-distinct peak is present. Because LCPs originate from many different sources and with much more copious yields than IMFs, the lack of a sideways peak does not exclude the presence of a shocklike component. Such effects may be buried in these ''inclusive'' results. In addition, if

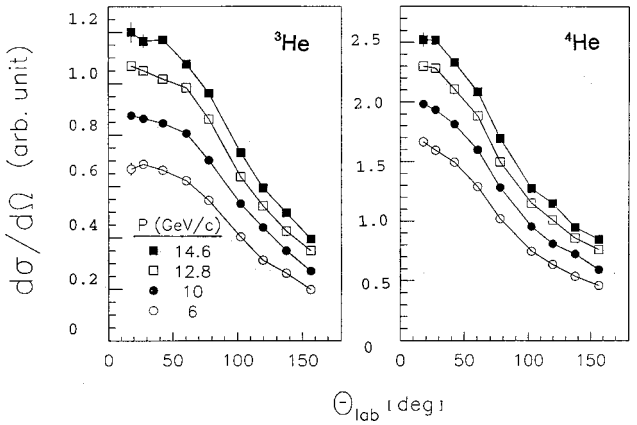

FIG. 3. ''Inclusive'' angular distributions for ^{3}He (left) and ^{4}He (right) emitted in proton-induced reactions on ^{197}Au. Beam momenta are indicated in the figure.

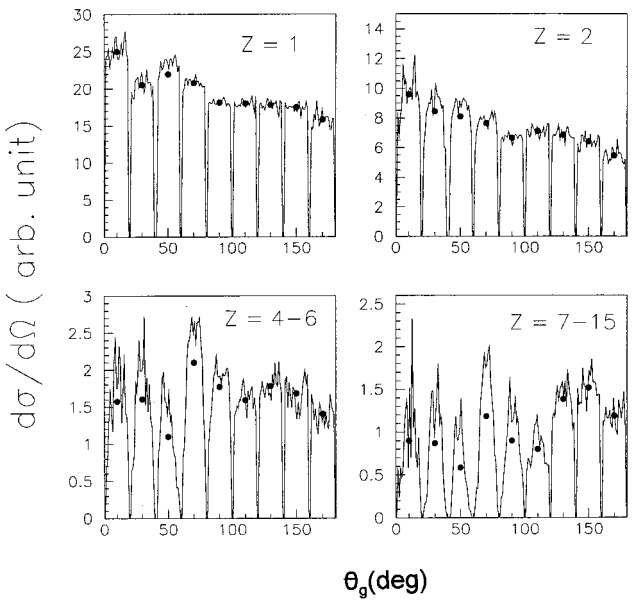

FIG. 4. Polar and azimuthal raw angular correlations $C(\theta\phi)$ for the trigger angle $\theta_t = 33° - 52°$ and beam momentum 14.6 GeV/c. Results are shown for IMFs in coincidence with protons, He ions, $Z = 4-6$ fragments, and $Z = 7-15$ fragments. Each slice represents an average polar angle θ_g corresponding to the nine rings in the ISiS array. Within each slice is the ϕ-dependent correlation for the eighteen detector telescopes in that polar-angle slice, ranging from $\langle\phi\rangle = 10°$ (first point) to 350° (last point). Dots give average value for each ring (polar angle).

such effects are present at angles less than 14°, the ISiS array would not detect them.

Focusing on the IMFs, the signature of a shock-wave or toroidal breakup mechanism would be the observation of events with enhanced fragment multiplicities in a localized angular interval; e.g., in an annulus about the beam axis or in a forward cone. To test this scenario, we have examined angular correlations between coincident IMFs. For reference, the ISiS array consists of nine annular rings, each corresponding to a fixed polar angle segment, (θ) and containing 18 azimuthal telescope segments (ϕ). In the analysis, gating conditions were set on the two polar-angle rings where the maximum in the angular distributions is observed, 33°–52° and 52°–69°, respectively. These are defined here as the ''trigger interval'' θ_t, and the IMFs as ''trigger fragments.'' For each of the 18 detector elements in these two polar-angle segments, the correlation with the remaining $(N_{\mathrm{IMF}}-1)$ fragments, θ_g and ϕ_g was determined; these fragments are defined as ''global fragments.'' The analysis here emphasizes the 14.6 GeV/c results, since the sideways peaking is most prominent at this momentum.

In Fig. 4 we show the raw correlations for the $\theta_t = 33° - 52°$ ring at 14.6 GeV/c beam momentum, gated on protons, He ions, $Z = 4-6$ and $Z \geqslant 7$ fragments, respectively. Each of the nine rings, corresponding to a given value of θ_g, is shown as a slice on each graph. Within each of the nine polar-angle slices, the correlation with the 18 azimuthal detectors is shown, ranging from centroids at 10° to 350° as one goes from left to right in each bin. The average correlation rate in each ring is indicated by the solid dot. No corrections for variations due to solid-angle differences, detector thicknesses and target shadowing near 90° have been applied to the results in Fig. 4.

The immediate message of Fig. 4 is the absence of any significant enhancement in the correlation probability for the trigger interval. As one examines the variations among the four types of trigger fragments in Fig. 4, there is a systematic evolution of the correlations with increasing fragment mass. For protons, the coincidence probability is nearly independent of either θ_g or ϕ_g, other than reflecting the angular distribution of these particles. Otherwise, the probability of observing an IMF in coincidence with a proton appears to be random. When He ions are the trigger, the dependence on θ_g is similar to that for protons. However, in the vicinity of the trigger detector, the dependence of the correlation probability on θ_g shows a decrease as one approaches the trigger detector. Again, the existence of multiple sources that produce LCPs complicates any interpretation of the global correlation pattern for these particles.

Examination of the IMF-IMF correlations shows several important features relevant to the question of dynamic production mechanisms. Most significant is the distinct suppression of the correlation yield within the trigger interval—as opposed to any enhancement that might signal a localized emission pattern. In addition, one notes that within the trigger interval there is a strong preference for correlated fragments to appear at an azimuthal angle 180° away from the trigger detector. As one moves to polar angles away from θ_t, this effect gradually diminishes so that in the backward hemisphere, the dependence on azimuthal angle ϕ_g is negligible. Thus, the conclusion of the IMF-IMF correlations is that in the vicinity of the trigger detector, the correlation probability is low, but as one moves to larger angles, the probability resembles a random distribution. This suggests that the IMF emission process is dominated by phase space and Coulomb effects, rather than by coherent dynamic processes such as shock waves or the breakup of residues with exotic shapes.

In order to investigate this conclusion further, the correlation for data with $N_{\mathrm{IMF}} \geqslant 3$ from the 14.6 GeV/c proton reaction have been normalized to a similar correlation analysis for the 5.0 GeV/c π^- data. For the reference correlation with the π^- beam, all events with NIMF$\geqslant$2 were accepted in order to insure comparison with a monotonically decreasing angular distribution (Fig. 1). This approach minimizes uncertainties due to solid angle, detector thresholds and target shadowing. As shown in Fig. 5, this analysis also fails to provide evidence for preferential emission of the fragments in any given angular region. The only obvious trend in Fig. 5 is the systematic increase in relative correlation probability with increasing angle, which arises from the more isotropic nature of the angular distributions as the beam momentum increases. Again, this supports the hypothesis that IMF emission is primarily influenced by Coulomb repulsion effects and global momentum conservation associated with the recoil nucleus and its fragmentation products.

In addition, a sphericity/coplanarity analysis [27] has been

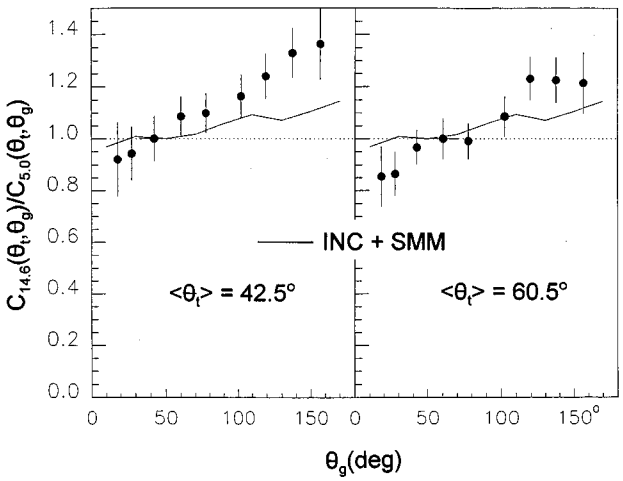

FIG. 5. Relative correlation probability (points) for coincident pairs of IMFs produced in $N_{\mathrm{IMF}} \geq 3$ events from the 14.6 GeV/c $p+^{197}$Au reaction, gated on the annular intervals 33°–52° (left) and 52°–69° (right). Correlations are normalized to an identical analysis for $N_{\mathrm{IMF}} \geq 2$ for the 5.0 GeV/c π^- data. IMF acceptance was $Z=4-12$ and $E/A=1-4$ MeV for the trigger and $Z=4-12$ and $E/A=1-8$ MeV for correlated IMFs. Solid line is the prediction of a hybrid INC/SMM [33] calculation.

performed on the 5.0 GeV/c π^- and 14.6 GeV/c proton data for thermal-like IMFs and light charged particles. The results are shown in Fig. 6. For the high IMF multiplicity events the average sphericity is $\langle S \rangle \sim 0.55$ and the coplanarity is $\langle C \rangle \simeq 0.10$. These values are nearly the same for both beam energies and are consistent with previous results for the 4.8 GeV ^{3}He$+^{197}$Au system, where no sideways peaking was observed [28,29]. No change in the coplanarity $\langle C \rangle$ is observed in the data, which might be expected if fissionlike

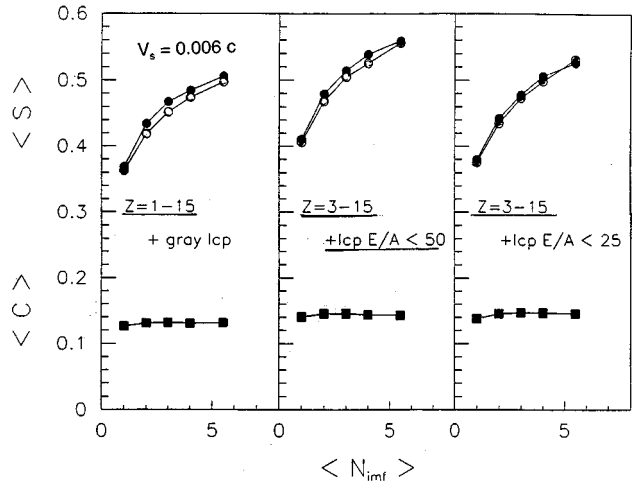

FIG. 6. Average event sphericity $\langle S \rangle$ and coplanarity $\langle C \rangle$ as a function of IMF multiplicity for events measured with a 14.6 GeV/c proton beam (solid points) and a 5.0 GeV/c π^- beam (open points). For the left-hand panel the fragment energy acceptance includes all detected fragments; the center panel limits acceptance to $E/A \leq 50$ MeV, and in the right-hand frame only ejectiles with $(E/A)_{\mathrm{IMF}} \leq 8$ MeV and $(E/A)_{\mathrm{LCP}} \leq 25$ MeV are accepted.

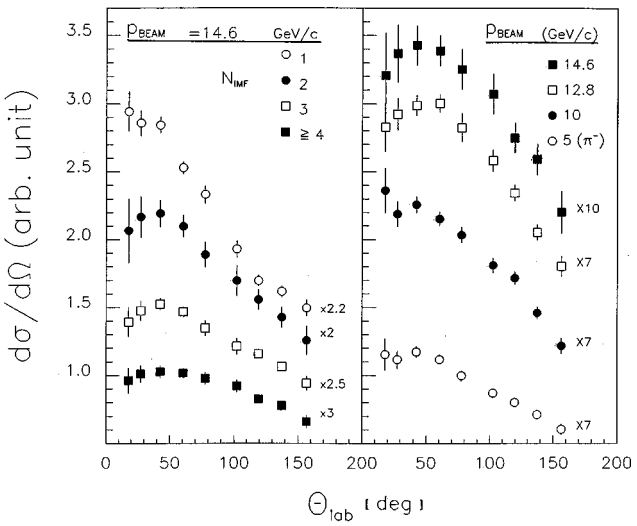

FIG. 7. Exclusive angular distributions of carbon fragments from a ^{197}Au target. Left-hand panel shows the dependence of the angular distributions on observed IMF multiplicity (see legend) for the 14.6 GeV/c $p+^{197}$Au system. Right-hand panel gives angular distributions gated on N_{IMF} 4 for the 5.0 GeV/c (open circles), 10.0 GeV/c p (solid circles), 12.8 GeV/c p (open squares), and 14.8 GeV/c p (solid squares). Relative cross sections as indicated by scale factors associated with each angular distribution.

events from a compact shape were present in significant yield. The multiplicity distributions for $E/A=1-4$ MeV ejectiles have also been compared for the same polar angle intervals in the forward and backward hemispheres. These are identical within statistics.

Thus, no statistically meaningful signature for dynamical production of IMFs due to a collective shock wave or breakup of a geometrically unstable configuration is apparent in the data. The two-body cleavage mechanism [14,15] is more difficult to assess in our data because of the multiplicity-three trigger condition and the 1 MeV/nucleon threshold of the ISiS array.

IV. ORIGIN OF SIDEWAYS PEAKING

In order to gain further insight into the origin of the sideways peaking effect, the dependence of the angular distributions on several exclusive properties has been investigated. The left panel of Fig. 7 shows the angular distributions for the 14.6 GeV/c proton beam as a function of the observed IMF multiplicity. For $N_{\mathrm{IMF}}=1$ the results are similar to those observed in the inclusive measurements for 6.0 GeV/c protons and 5.2 GeV/c pions. As the IMF multiplicity increases, the sideways peak develops and shifts to larger angles. In addition, the ratio of the peak yield to that at the backward-most angle decreases from about 2.0 to 1.5. Similar trends are observed for the 12.8 and 10.0 GeV/c beams, although less pronounced. Thus, the sideways peaking effect is clearly associated with high deposition-energy multifragmentation events.

In the right-hand panel of Fig. 7 the angular distributions are shown for the gating condition $N_{\mathrm{IMF}} \geq 4$ for the

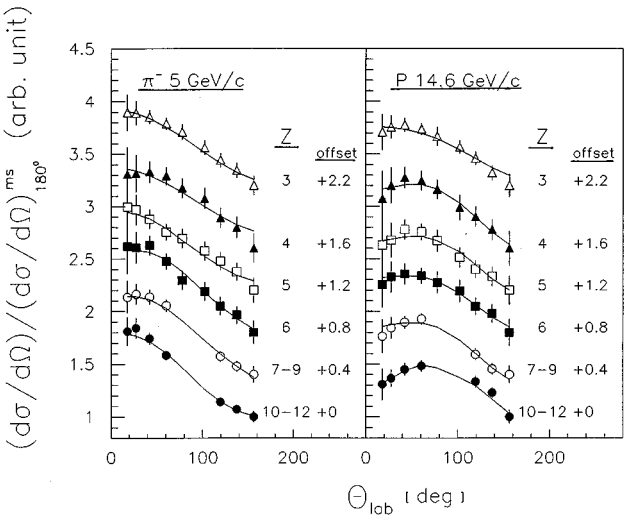

FIG. 8. Exclusive angular distributions for $N_{\mathrm{IMF}} \geqslant 4$ gated on IMF charge (see legend) for the 5.0 GeV/c bombardment (left) and 14.6 GeV/c p bombardment (right). Offset values at right of each curve have been added to the corresponding ordinate value for ease in making relative shape comparisons; i.e., all curves are normalized to 1.0 at 180° on the basis of moving-source fits (solid lines) and do not represent relative cross sections. For $Z>6$ the points near 90° are omitted because of target-shadowing effects.

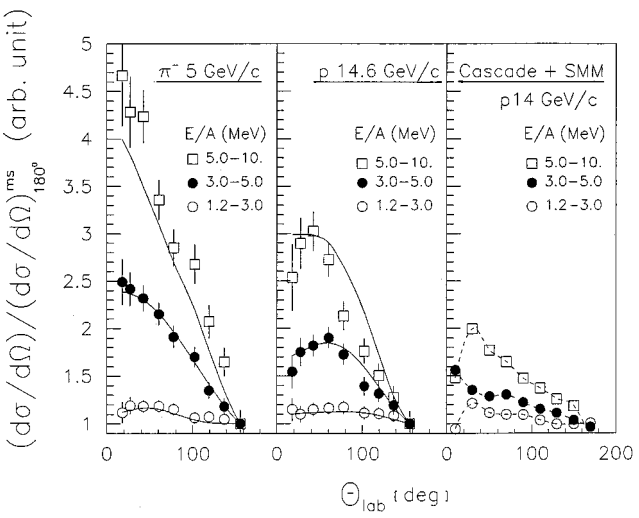

FIG. 9. Dependence of relative angular distributions on IMF kinetic energy for $Z=5-9$ fragments formed in events with IMF multiplicity $\geqslant 4$ for 5.0 GeV/c (left) and 14.6 GeV/c proton (right) beams incident on ^{197}Au. Angular distributions are normalized to 1.0 at 180°. Energy bins are indicated in the figure. Solid lines in left and center panels are results of moving-source fits. Right-hand panel shows prediction of INC/SMM calculation [33] for the 14 GeV/c $p+^{197}$Au reaction, binned the same as the data.

5.0 GeV/c π^- and 10.0, 12.8, and 14.6 GeV/c proton beams. Here one observes the same systematic trend as the inclusive data in Fig. 1, with the peak shifted toward larger angles. For the 5.0 GeV/c π^- case, selecting high multiplicity events leads to a flattening of the angular distribution at forward angles.

The influence of IMF charge on the angular distributions is presented in Fig. 8 for the 5.0 GeV/c π^- and 14.6 GeV/c proton bombardments. Both cases show $N_{\mathrm{IMF}} \geqslant 4$ data only. In order to permit a comparison of the angular-distribution shapes, a moving-source fit has been performed, given by the solid lines in Fig. 8. The fit angular distribution for each charge has then been normalized to 1.0 at the backward-most angle. Offset values, shown to the right of each angular distribution, have been added to the ordinate for each point in order to provide a basis for relative comparisons as a function of Z. For the 5.0 GeV/c π^- case, the forward-peaked angular distributions exhibit nearly identical slopes for all IMF Z values. In contrast, at 14.6 GeV/c there is a distinct evolution of the peak angle toward larger polar angles, as well as a weak trend toward greater isotropy as the IMF charge increases. This effect has also been noted in inclusive studies [3,8], as well as for heavier fragments in heavy-ion measurements [30]. Thus, the heavier fragments appear to feel the focusing mechanism more strongly.

The most striking feature of the exclusive angular distributions is the dependence on IMF kinetic energy. Figure 9 shows the relative angular distributions of $Z=5-9$ fragments with energy cuts of $E/A=1.2-3$, 3–5, and 5–10 MeV, respectively, imposed on the spectra. Data are shown for 5.0 GeV/c π^- (left) and 14.6 GeV/c proton beams (center) for $N_{\mathrm{IMF}} \geqslant 3$, normalized to 1.0 at the backward-most point. It should be emphasized that these are relative angular distributions; the IMF yield is actually largest for the lowest E/A bin. This plot demonstrates that as the IMF velocity decreases, the maximum differential cross section evolves towards more backward angles and the overall angular distribution becomes more isotropic.

The observation that sideways emission is favored by high IMF mass and low IMF kinetic energies suggests a possible kinematic origin for the peaking effect. The diffractive nature of the initial *N-N* collision preferentially produces a secondary nucleon or N^* that recoils at 70°–90° to the beam [31]. Thus, subsequent dissipation during the cascade imparts a significant transverse velocity to the heavy residue. This is supported by intranuclear cascade calculations (INC) [32,33] in Fig. 10, performed for random impact parameters. Here the distribution of longitudinal versus transverse velocity ($v_\parallel$ vs $v_\perp = \sqrt{v_x^2+v_y^2}$) is plotted for recoils with excitation energies $E^*>50$ MeV produced in the 1.3, 4.0, and 14.6 GeV/c $p+$Au reaction and for the 14.0 GeV/c case for $E^*>800$ MeV.

The simulation results in Fig. 10 show that at 1.3 GeV, both the longitudinal and perpendicular velocities are small (~0.10 cm/ns), with approximately equal magnitudes. As the beam energy increases, one observes both a significant spreading of the recoil velocity distribution in $v_\parallel$ vs $v_\perp$ space and an increase in $v_\perp$ relative to $v_\parallel$. For the 14 GeV case, transverse velocities up to 1 cm/ns are predicted for the heavy residues. In addition, a significant fraction of the residues recoil into the backward hemisphere. This is illustrated in Fig. 11, where the predicted distribution of total recoil velocity versus recoil angle is plotted for the $p+^{197}$Au reaction at 1.3 and 14.0 GeV. In both cases, the spread in

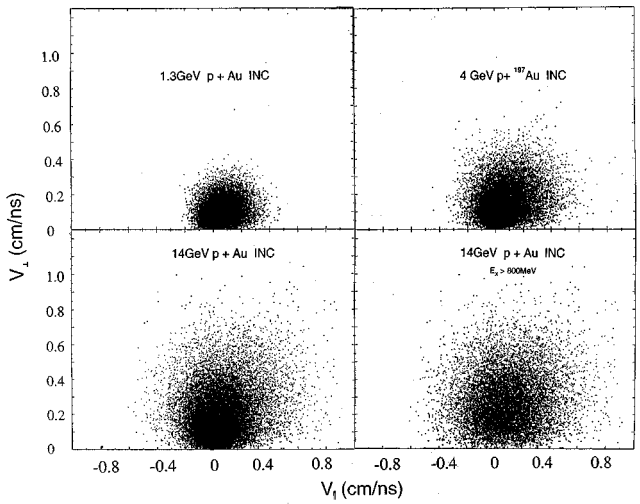

FIG. 10. Intranuclear cascade calculations [32] showing the distribution of longitudinal versus perpendicular velocity for residues with $E^*>50$ MeV formed in the $p+^{197}$Au reaction at incident energies of 1.3 GeV (upper left), 4 GeV (lower left), and 14 GeV (upper right). The panel at the lower right shows the effect at 14 GeV of gating on excitation energies >800 MeV.

recoil angle is very broad. However, at 1.3 GeV the recoil angular distribution is predominantly in the forward hemisphere, whereas at 14 GeV the distribution is much more isotropic. For high deposition energies ($E^*>800$ MeV) these effects are even more pronounced, also shown in Fig. 11.

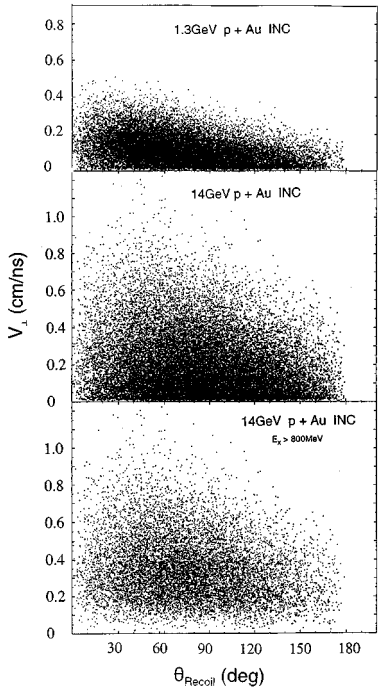

FIG. 11. Recoil velocity as a function of recoil angle predicted by INC calculation [32] for reactions on ^{197}Au induced by 1.3 GeV p (top), 14 GeV p (middle), and 14 GeV p with $E^*>800$ MeV (bottom).

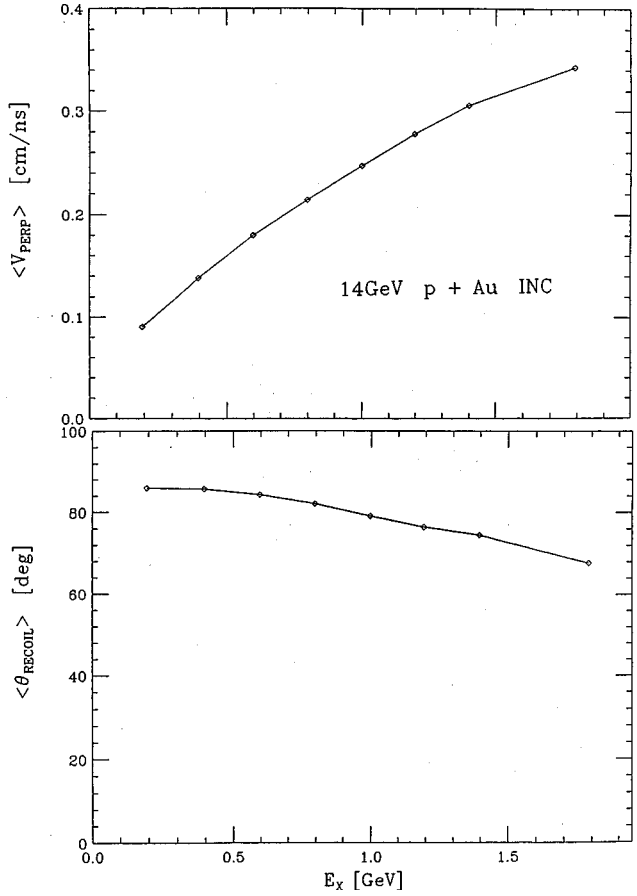

FIG. 12. INC predictions [32] of the average perpendicular velocity (top) and average recoil angle (bottom) as a function of excitation energy for the 14 GeV $p+^{197}$Au reaction.

The predicted dependence of the average recoil velocity v_R and angle θ_R on residue excitation energy for the 14-GeV $p+^{197}$Au reaction is shown in Fig. 12. The INC simulation illustrates that, on average, high excitation energies are associated with large perpendicular velocity components. There is also a slight decrease in the average recoil angle with increasing excitation energy, but even for the most violent events, the average recoil is focused into the angular range above 60°. While the average values of $\langle v_R \rangle$ are relatively small, the widths of the distributions are quite large, as evidenced in Figs. 10 and 11. The impact of this transverse focusing of the recoils on the IMF angular distributions will be greatest for those recoils with the highest v_R values (and excitation energies) that emit low-velocity IMFs; that is, those events with high multiplicity (Fig. 7), large IMF charge (Fig. 8) and low kinetic energy (Fig. 9). For example, the lowest kinetic energy bin in Fig. 9 corresponds to a velocity range $v_{\mathrm{IMF}}=1.5-2.5$ cm/ns—and it is these events that exhibit the largest fraction of the multifragmentation cross section in hadron-induced reactions.

While sideways peaking can be explained in terms of the focusing effect associated with large transverse recoil velocities, the question remains as to why this feature of the angular distributions only appears above hadron beam energies in the range of 5–10 GeV. In Fig. 13, we show INC predictions

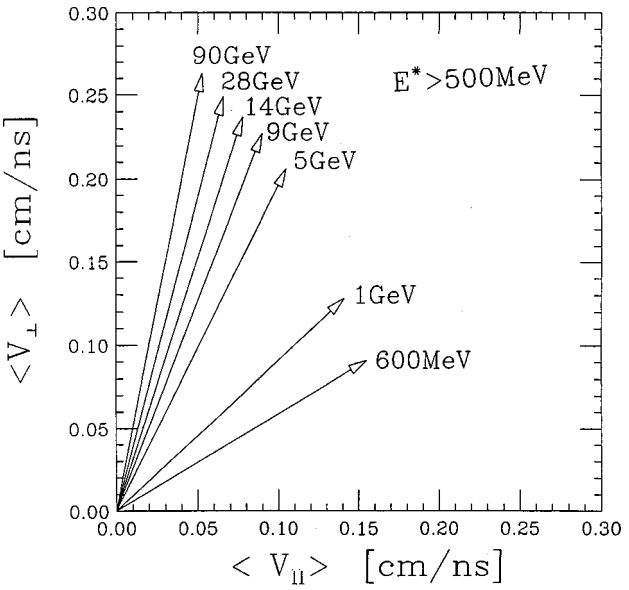

FIG. 13. INC predictions [32] of the average perpendicular velocity versus the average longitudinal velocity for the $p+^{197}$Au reaction. Incident beam energies are indicated on the figure.

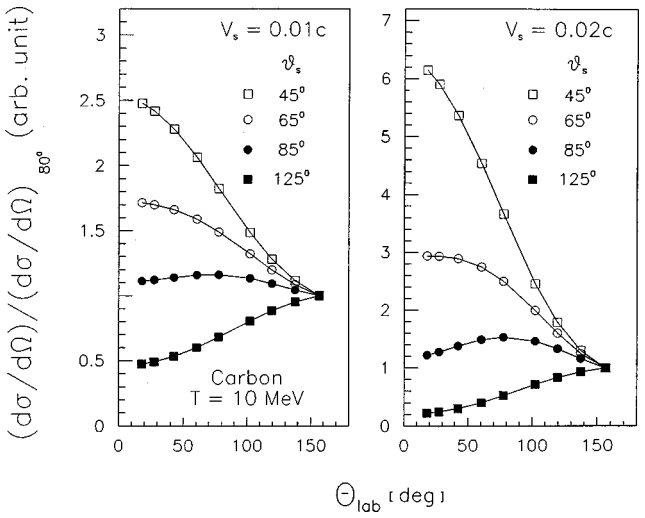

FIG. 14. Simulations of angular distributions for carbon fragments emitted from a residue at a temperature of $T=10$ MeV, assuming various recoil angles for the source, as indicated on the figure. Two source velocities are shown, $0.01c$ (left panel) and $0.02c$ (right panel). All angular distributions are normalized to 1.0 at 180°.

of the average velocity vector $\langle v_R \rangle$ for residues with $E^* > 500$ MeV produced in reactions of 600 MeV to 90 GeV hadron beams with ^{197}Au. With increasing beam energy, $v_\perp$ becomes increasingly important. The most rapid growth occurs between 1.0–5.0 GeV, followed by a nearly constant value above 10 GeV.

To investigate the influence of collision kinematics on the IMF angular distributions, we have performed a Monte Carlo simulation for a one-component moving-source that emits fragments from a Au-like residue moving at a fixed angle θ_s with respect to the beam. The simulation assumes isotropic emission in the source frame from residues with temperature $T=10$ MeV and recoil velocities of $0.01c$ and $0.02c$. The results for carbon fragments are shown in Fig. 14. For residue recoil angles of about 60° or less, only a monotonically-decreasing angular distribution results; i.e., no sideways peaking. This is consistent with the observation of such angular distributions at incident energies below 5 GeV, where the INC simulations predict smaller recoil momenta for residues emitted at more-forward angles. On the other hand, once the most probable recoil angle evolves beyond about 60°, the coupling of the residue and the IMF velocity vectors produces sideways-peaked angular distributions. Thus the distribution of recoil angles for the residues strongly influences the probability for sideways peaking in the laboratory system.

We have also performed a simple two-component moving-source fit to the measured spectra, assuming one source is moving in the beam direction and the second is focused at some average transverse angle, determined by the fit. Both sources assume isotropic emission in the source frame. The fits are shown as the solid lines in the first two panels of Fig. 9 for fragments emitted from $N_{\rm IMF}\geqslant 4$ events for the 5 GeV/c π^- and 14.6 GeV/c proton reactions. Figure 15 shows these fits to the carbon spectra and angular distributions. In Fig. 16 the fits to the angular distributions, gated on fragment energy for boron fragments are presented. The transverse source accounts for about 80% of the yield at the higher beam momentum, but only about 25% for the lower beam momentum. This fit yields an average recoil angle of ~80° for the 14.6 GeV/c data and a longitudinal-source velocity of $v\sim 0.006c$. Combined, the two sources give a satisfactory fit to the data.

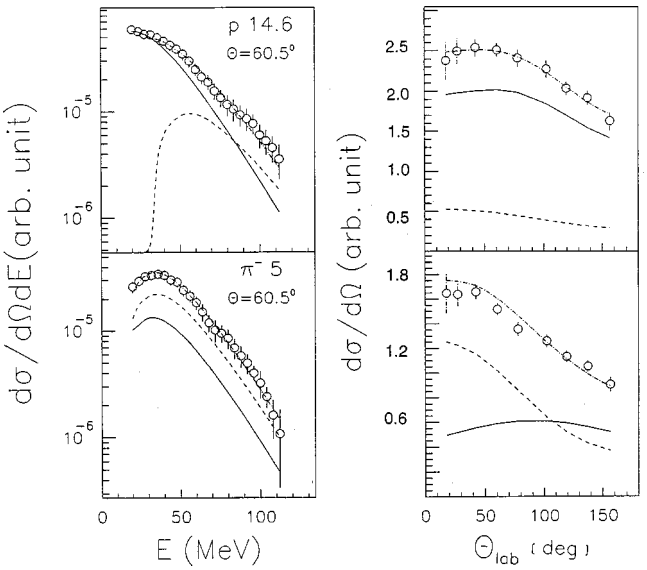

FIG. 15. Moving-source fits to energy spectra for carbon fragments at 60.5° (left panels) and angular distributions (right panels) for the 14.6 GeV/c (top) and 5.0 GeV/c reactions (bottom). Two sources are assumed, one parallel to and the other perpendicular to the beam axis. Data (open points) are for carbon fragments and $N_{\rm IMF}\geqslant 4$. Dashed line is the longitudinal source, solid line is the perpendicular source, and broken line is the sum of these.

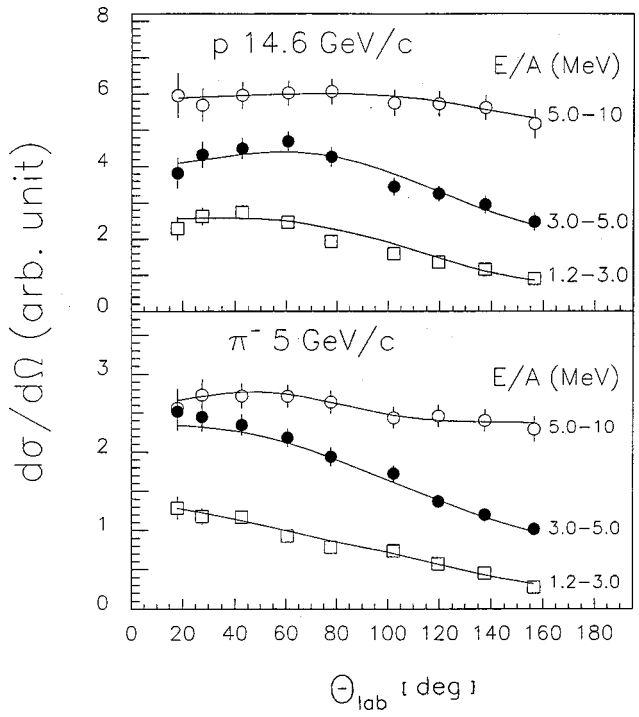

FIG. 16. Moving source fits (solid lines) to energy-gated angular distributions for $Z=5-9$ fragments, as in Fig. 16. IMF energy interval is indicated in the figure for each set of data points.

To simulate the combined effects of recoil angle and statistical breakup, we have also examined the angular distributions predicted by a hybrid intranuclear cascade statistical multifragmentation model [33]. Such a model should provide a schematic picture of the combined influence of the fast cascade and statistical multifragment breakup on the angular distributions. We have summed all IMFs with $Z=5-9$ to improve statistics. The model predictions are compared with the relative correlation results in Fig. 5, normalized to each of the trigger angular intervals. A qualitative consistency is observed. The inclusion of forward-peaked nonequilibrium light-charged-particle and IMF emission in the model would improve the agreement.

The angular distributions predicted by the INC/SMM model for IMFs with $E/A=1.2-3$, 3–5, and 5–10 MeV are compared with the data in the right-hand panel of Fig. 9. The latter comparison demonstrates that significantly greater isotropy is expected for the low-energy IMFs relative to those with higher energies. Accounting for prebreakup IMF emissions ($\sim$10–15 % of the yield) would further increase the forward peaking of the most energetic component. These same arguments serve to explain the increase in the peak angle as a function of IMF charge, since the average velocity of the fragments decreases with increasing Z. Thus, the simulation is consistent with a two-step mechanism in which a sideways peak in the angular distributions is produced by kinematic focusing of IMFs emitted from a hot residue with significant transverse momentum.

V. CONCLUSIONS

In summary, we have performed exclusive studies that investigate the origin of sideways peaking of IMFs produced in hadron-heavy nucleus collisions. The effect becomes prominent above about 10 GeV/c beam momentum and is found to be most pronounced for high-multiplicity, low kinetic-energy multifragmentation events. The peak angle increases with increasing beam energy and IMF charge. Investigations of IMF-IMF angular correlations, multiplicity distributions, and sphericity and coplanarity distributions provide no ''smoking gun'' that would support arguments for dynamical effects such as shock waves or the breakup of exotic geometric shapes. Instead, it appears that the sideways peaking of IMFs can be largely explained by kinematic-focusing effects associated with statistical/thermal multifragmentation of a hot residue having a significant velocity component transverse to the beam axis. This is consistent with the observation that all other multifragmentation observables are insensitive to beam energy above about 5 GeV. Thus, if dynamical effects are present in the IMF data, they exist on a background in which kinematic focusing of heavy recoils cannot be ignored.

ACKNOWLEDGMENTS

The authors wish to thank V. D. Toneev for providing a version of his QGSM code and Wolfgang Bauer, Pawel Danielewicz and Scott Pratt for valuable discussions concerning these results. The assistance of Hugh Brown, John Gould, Bill McGahern, and Phil Pile at AGS was vital to the successful completion of these experiments. We also thank Bill Lozowski at IUCF for fabricating the targets. One of us (W.A.F.) acknowledges the support of the Indiana University Institute for Advanced Study. Support for this research was provided by the U.S. Department of Energy, the National Science Foundation, the National Sciences and Engineering Research Council of Canada, and the Robert A. Welch Foundation.

[1] J. B. Cumming, R. J. Cross, Jr., J. Hudis, and A. M. Poskanzer, Phys. Rev. **134**, B167 (1964).

[2] J. Hudis, in *Nuclear Chemistry*, edited by L. Yaffe (Academic Press, New York, 1998), p. 169.

[3] L. P. Remsberg and D. G. Perry, Phys. Rev. Lett. **35**, 361 (1975).

[4] A. M. Poskanzer, G. W. Butler, and E. K. Hyde, Phys. Rev. C **3**, 882 (1971).

[5] R. E. L. Green and R. G. Korteling, Phys. Rev. C **22**, 1594 (1980).

[6] G. D. Westfall, R. G. Sextro, A. M. Poskanzer, A. M. Zebelman, G. W. Butler, and E. K. Hyde, Phys. Rev. C **17**, 1368 (1978).

[7] D. R. Fortney and N. T. Porile, Phys. Lett. **76B**, 553 (1978).

[8] J. Urbon, S. B. Kaufman, D. J. Henderson, and E. P. Steinberg, Phys. Rev. C **21**, 1048 (1980).
[9] N. Porile *et al.*, Phys. Rev. C **39**, 1914 (1989).
[10] W.-c. Hsi *et al.*, Phys. Rev. Lett. **79**, 817 (1997).
[11] S. J. Yennello *et al.*, Phys. Rev. C **41**, 79 (1990).
[12] A. E. Glassgold, W. Heckrotte, and K. M. Watson, Ann. Phys. (N.Y.) **6**, 1 (1959).
[13] K. Gottfried, Phys. Rev. Lett. **32**, 957 (1974); *Proceedings of the 5th International Conference on High Energy Physics and Nuclear Structure*, edited by G. Tibell (North-Holland, Amsterdam, 1994), p. 79.
[14] B. D. Wilkins, S. B. Kaufman, and E. P. Steinberg, Phys. Rev. Lett. **43**, 1080 (1979).
[15] J. Hüfner, Phys. Rep. **124**, 130 (1985); S. Bohrmam, J. Hüfner, and M. C. Nemes, Phys. Lett. **120B**, 59 (1983).
[16] K. H. Tanaka *et al.*, Nucl. Phys. **A583**, 581c (1995).
[17] T. Maruyama and K. Nitia, Prog. Theor. Phys. **97**, 579 (1997).
[18] P. J. Siemens and H. Bethe, Phys. Rev. Lett. **18**, 704 (1967).
[19] C. Y. Wong, Ann. Phys. (N.Y.) **77**, 279 (1973).
[20] W. Bauer, G. F. Bertsch, and H. Schulz, Phys. Rev. Lett. **69**, 1888 (1992).
[21] L. G. Moretto, K. Tso, N. Colonna, and G. J. Wozniak, Phys. Rev. Lett. **69**, 1884 (1992).
[22] H. M. Xu, C. A. Gagliardi, R. E. Tribble, and C. Y. Wong, Nucl. Phys. **A569**, 575 (1994).
[23] G. Wang, K. Kwiatkowski, V. E. Viola, W. Bauer, and P. Danielewicz, Phys. Rev. C **53**, 1811 (1996).
[24] M. Colonna *et al.*, Phys. Rev. C **55**, 1404 (1997).
[25] W.-c. Hsi *et al.*, Phys. Rev. C **58**, R13 (1998).
[26] K. Kwiatkowski *et al.*, Nucl. Instrum. Methods Phys. Res. A **360**, 571 (1995).
[27] G. Fai and J. Randrup, Nucl. Phys. **A404**, 551 (1983); J. A. Lopez and J. Randrup, *ibid.* **A491**, 477 (1989).
[28] E. Renshaw Foxford *et al.*, Phys. Rev. C **54**, 749 (1996).
[29] K. B. Morley *et al.*, Phys. Rev. C **54**, 737 (1996).
[30] W. Loveland, K. Aleklett, R. Yanez, A. Srivastava, and J. O. Liljenzin, Phys. Lett. B **312**, 53 (1993).
[31] H. Araseki and T. Fujita, Nucl. Phys. **A399**, 434 (1983).
[32] V. Toneev, N. S. Amelin, K. K. Gudima, and S. Yu. Sivoklokov, Nucl. Phys. **A519**, 463c (1990).
[33] A. Botvina, A. S. Iljinov, and I. N. Mishustin, Nucl. Phys. **A507**, 649 (1990).